EPS-SG Windscatterometer Concept Tradeoffs and Wind Retrieval Performance Assessment

Chung-Chi Lin, Maurizio Betto, Maria Belmonte Rivas, Ad Stoffelen, and Jos de Kloe

***Abstract*—The EUMETSAT Polar System-Second Generation (EPS-SG) mission will be deployed in the 2019–2020 timeframe in order to ensure continuity of the EPS observation missions, currently realized with the *MetOp* satellite series, to support *operational meteorology and oceanography*; in particular, for numerical weather prediction (NWP), *climate monitoring* and to develop new *environmental services*. The scatterometer (SCA) is one of the high-priority payload instruments to provide vector surface wind observations over the ocean, which constitute an important input to NWP, as well as valuable information for tracking of extreme weather events. The EPS-SG SCA shall offer observations with higher spatial resolution than those provided by ASCAT on board *MetOp*, operating at C-band and with VV polarization. Furthermore, addition of HH or VH polarization is considered as an option. Phase 0 industrial studies, addressing the complete system design, have taken place from 2008 to 2009. Two study teams, constituted, respectively by Astrium SAS and Thales Alenia Space Italy, have performed comprehensive analyses of the system requirements, tradeoffs of various concepts, and preliminary design of the selected concepts, which included both the single and dual satellite configurations. Three distinct SCA concepts were initially considered for tradeoffs: 1) fixed fan-beam concept with six fixed antennas; 2) rotating fan-beam concept with a single rotating antenna; 3) rotating pencil-beam concept. The first two concepts were further elaborated during Phase 0, and the fixed fan-beam concept was selected as baseline after a final tradeoff. For supporting the above instrument concept elaboration by the industrial study teams during Phase 0, the Royal Dutch Meteorological Institute (KNMI) has developed retrieval algorithms tailored to those concepts, derived from the ASCAT operational algorithms, and specific metrics to characterize the associated retrieval performance. The metrics used for the present performance assessment were: 1) wind vector root-mean-square error; 2) ambiguity susceptibility; and 3) wind biases. The end-to-end performance evaluation makes use of an ensemble of wind fields as input having the mean climatology distribution, generates the output wind-fields which account for the measurement system imperfections and geophysical noise, and computes the performance metrics for comparisons. This paper describes the three SCA concepts as analysed in Phase 0 studies by the industrial study teams and summarizes the technical tradeoffs carried out. The performance metrics are described and applied to two of the concepts in order to compare their respective merits. It is shown that both concepts are able to meet the observation requirements of EPS-SG.**

***Index Terms*—EUMETSAT polar system (EPS), EPS-second generation (EPS-SG), ocean wind, windscatterometer, wind retrieval.**

I. Introduction

THE EUMETSAT polar system (EPS) is a meteorological data acquisition system based on the *MetOp* series of low-earth orbiting satellites. A successor program, EPS-second generation (SG), will replace EPS in the 2019–2020 timeframe [1], [2]. The scatterometer (SCA) is one of the high-priority payload instruments to provide vector surface wind observations over the ocean which constitute an important input to NWP as well as valuable information for tracking of extreme weather events. The secondary products derived from the SCA data are

- land surface soil moisture;
- leaf area index;
- snow water equivalent;
- snow cover;
- sea-ice type;
- sea-ice extent.

The EPS-SG SCA shall offer observations with higher spatial resolution (two-fold increase) and radiometric stability than those provided by ASCAT on board *MetOp*. The resolution improvement, at the same time maintaining the radiometric performance achieved by ASCAT, is necessary for providing better observation of coastal winds, frontal systems, tropical cyclones, and for discriminating rain-affected pixels. As the measurements with VV polarization of ASCAT is known to saturate above 25 m/s, addition of HH or VH polarization is considered as an option for extending the upper measurement dynamic range.

Two parallel Phase 0 industrial studies, contracted, respectively to Astrium SAS and Thales Alenia Space Italy, addressing the complete system design, have taken place from 2008 to 2009. Following the system tradeoffs made and conclusions at the end of Phase 0, a two-satellite configuration will be assumed for phase A/B1 studies. In this scenario, the mission will be implemented with a sequence of identical pairs of EPS-SG satellites (Satellites A1 and B1, followed by Satellites A2 and B2, etc.), with payload instruments distributed appropriately on the two satellites (A and B), taking into account constraints imposed by the coregistration requirements among some of them.

Three distinct SCA concepts were initially considered. 1) a fixed fan-beam concept with six fixed antennas; 2) a rotating fan-beam concept with a single rotating antenna [3]; and 3) a rotating pencil-beam concept. The two first concepts were further elaborated in Phase 0 following a preliminary tradeoff of the three concepts.

Manuscript received February 20, 2011; revised August 5, 2011 and October 10, 2011; accepted November 19, 2011.

C.-C. Lin and M. Betto are with the European Space Agency-ESTEC, 2200 AG Noordwijk, The Netherlands (e-mail: Chung-Chi.Lin@esa.int; Maurizio.Betto@esa.int).

M. Belmonte Rivas is with the National Center for Atmospheric Research, Boulder, CO 80301 USA (e-mail: rivasm@ucar.edu).

A. Stoffelen and J. de Kloe are with the Royal Netherlands Meteorological Institute (KNMI), 3732 GK De Bilt, The Netherlands (e-mail: ad.stoffelen@knmi.nl; Jos.de.Kloe@knmi.nl).

Digital Object Identifier 10.1109/TGRS.2011.2180393

TABLE I

Frequency	5.3 GHz
Polarization	VV as baseline (+ HH or VH on a reduced set of beams as option)
Number of azimuth views	≥ 3, ideally separated by 45° each (azimuth diversity req.)
Incidence angle	$\theta_i \geq 20°$
Dynamic range	4 – 25 m/s (≤ 40 m/s in case of HH or VH implementation)
Horizontal resolution	25 km × 25 km
Horizontal sampling	12.5 km × 12.5 km
Radiometric resolution	≤ 3 % for $\theta_i \leq 25°$ at 4 m/s cross-wind ≤ $(0.175 \times \theta_i - 1.375)$ % for $\theta_i > 25°$ at 4 m/s cross-wind ≤ 3 % at 25 m/s up-wind
Radiometric stability	≤ 0.1 dB
Absolute radiometric bias	≤ 0.35 dB peak-to-peak per beam
Coverage	≥ 97 % in 48 hours

For supporting the above instrument concept elaboration by the industrial study teams during Phase 0, Royal Netherlands Meteorological Institute (KNMI) has developed retrieval algorithms tailored to the concepts (1) and (2), derived from the ASCAT operational algorithms, and specific metrics to characterize the associated wind retrieval performance. Those algorithms and metrics are also applied to SeaWinds/QuickSCAT [4] for illustrating the wind retrieval procedure.

II. Scatterometry Technical Requirements

The SCA payload is real-aperture, pulsed imaging radar which measures the normalized (per-unit-surface) radar backscatter coefficient of the ocean surface (called "σ^0") over a swath. The swath is divided into regularly spaced wind vector cells (WVCs) in along- and across-track directions, and each WVC is imaged at a number of azimuth view angles from the satellite as it flies past the target area (called "azimuth views" for the remaining of the paper). At least three such azimuth views per WVC are required, ideally separated by 45° each in azimuth in order to enable vector wind determination under optimum condition (azimuth diversity requirement). A large number of independent looks are summed in range and azimuth (multilooking) over each WVC for forming an azimuth view in order to achieve the specified radiometric resolution of the σ^0 estimate. The set of σ^0 measurements are uniquely related to the 10-m vector wind over the WVC through the geophysical model function (GMF) [5]. The wind inversion is based on a search for minimum distances between the measured set of σ^0s and all the backscatter model solutions lying on the GMF surface, taking into account instrumental and geophysical noise sources [6]. A combination of measurement noise and GMF degeneracy will usually lead to multiple and equally likely solutions (wind ambiguities), which have to be filtered out using the background wind information provided by a NWP model to initialize an ambiguity removal process.

The main technical requirements of SCA as specified by the EPS-SG users [7] are summarized in Table I.

The overriding requirement of SCA is to ensure continuity of observations currently provided by ASCAT operating at C-band (5.3 GHz) and with VV polarization. The major improvements

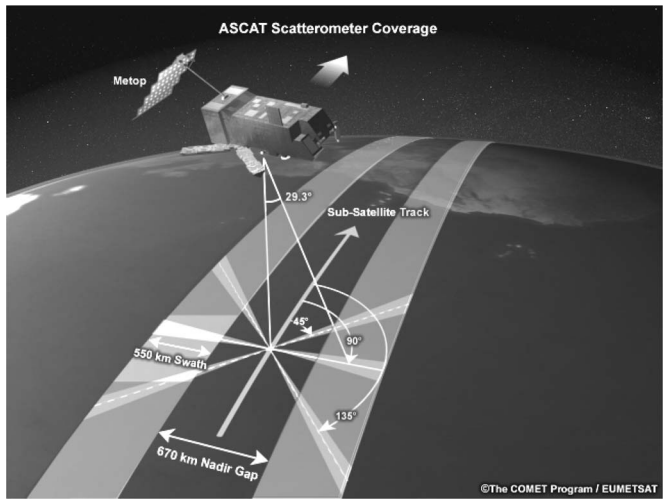

Fig. 1. ASCAT measurement geometry (fixed fan-beam scatterometer).

to be brought by SCA with respect to ASCAT are the spatial resolution of 25 km × 25 km (two-fold increase) and the radiometric stability of ≤ 0.1 dB. Furthermore, HH or VH polarization measurements on a subset of beams are desirable as options for extending the upper dynamic range of wind observation. As a matter of fact, recent observations seem to indicate that radar backscatter of the ocean would saturate at much higher wind speeds with HH or VH polarization [8], [9], whereas the response with VV polarization seems to saturate at 25 m/s. No sufficiently validated GMFs for HH and VH at C-band are yet available, and their determination is a subject of future measurement campaigns.

III. Instrument Concept Tradeoffs

Three distinct instrument concepts were considered at the start of Phase 0.

1) fixed fan-beam SCA (e.g., ASCAT, ERS-SCAT, NSCAT);
2) rotating fan-beam SCA (e.g., RFSCAT [3]);
3) rotating pencil-beam SCA (e.g., SeaWinds/QuickSCAT [4]).

A. Fixed Fan-Beam Concept

The fixed fan-beam concept has a strong heritage from ASCAT with excellent radiometric performance and good coverage. The observation geometry (Fig. 1) is optimum over the whole swath in terms of azimuth diversity with three views (45°, 90°, and 135° w.r.t. subsatellite track), maximizing the wind directional sensitivity. This observation geometry results in a nearly uniform wind retrieval performance over the swath when the radiometric performance is appropriately scaled with incidence angle (see the radiometric resolution requirement in Section II). One major drawback of this concept is the unavoidable observation gap at nadir, which is as large as 670 km for ASCAT. This can be reduced to 520 km when the minimum incidence angle is reduced to 20°, below which the wind directional sensitivity is seriously degraded in the GMF.

In the low incidence range (20° to 25°), about 1000 to 2000 independent looks have to be averaged in order to achieve

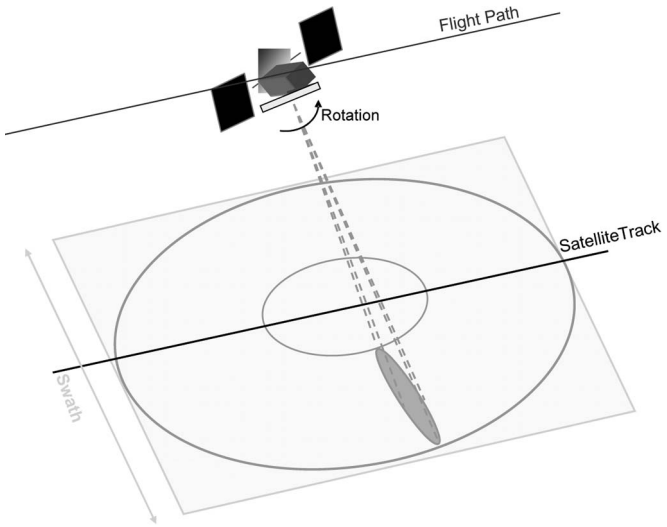

Fig. 2. Rotating fan-beam scatterometer.

a radiometric resolution of 3% [see (2)] with a signal-to-noise ratio (SNR) of 1 or larger. With the beams fixed at constant azimuth angles, a large number of pulse echoes can be incoherently averaged in the along-track direction over a given WVC, which is proportional to the radar pulse repetition frequency (PRF). This high number of along-track looks results in a low number of range looks needed to meet the radiometric resolution requirement, leading to a lower bandwidth and hence a reasonable RF power even with low gain of fan-beam antennas. The concept nevertheless requires six antennas in order to cover both sides of the subsatellite track, together with a beam-switching matrix. In addition, a subset of the antennas has to be stowed for launch and deployed in orbit.

The antenna length will have to be increased with respect to that of ASCAT in order to meet the horizontal resolution requirement (see Section IV). Due to the increased system bandwidth necessary to achieve the required number of looks within the 25 km $\times$ 25 km resolution cell (ASCAT resolution is 50 km $\times$ 50 km), a higher RF power than that of ASCAT is also needed. Three possible pulsed concepts were considered: 1) a long modulated pulse, low PRF concept (ASCAT heritage); 2) a short modulated pulse, high PRF concept; 3) a short unmodulated pulse, high PRF concept (ERS-SCAT heritage). All three concepts are feasible, resulting in a similar total dc power budget of 340 to 380 W.

B. Rotating Fan-Beam Concept

The rotating fan-beam SCA (Fig. 2) makes use of a single fan-beam antenna rotated around a nadir axis with a speed of approximately 2–3 r/min. The initial concept was studied and performance assessed by Lin *et al.* [3], [10], [11]. The slow rotation of the antenna, combined with the range gating of the radar echo, results in multiple azimuth views of a given WVC during a satellite pass. As opposed to the fixed fan-beam concept, the number of azimuth views varies across the swath and is a function of the rotation speed. The azimuth diversity degrades around nadir and at the swath edges due to the scanning geometry. Thus, despite the continuous coverage by the antenna beam, the wind retrieval performance degrades in those regions due to the reduced azimuth diversity.

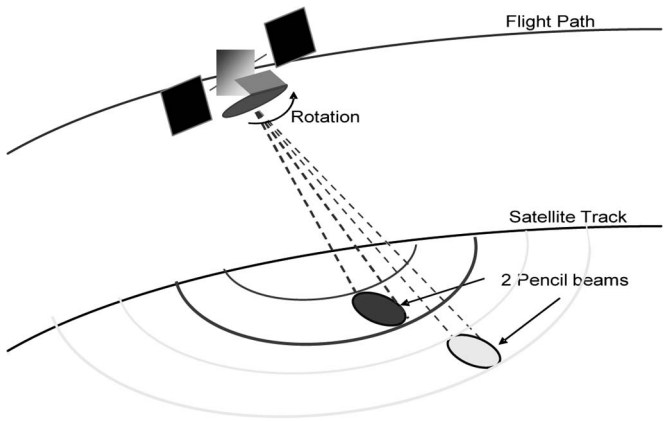

Fig. 3. Rotating pencil-beam scatterometer.

Nevertheless, a performance comparable to that of the fixed fan-beam concept can be achieved between the stand-off distances from the subsatellite track of 100 and 800 km (see Section V) for scan speeds larger than 2 r/min, with a nadir region of 200 km where the performance is degraded. The antenna length necessary for achieving the required spatial resolution is similar to that of the mid-antenna of the fixed fan-beam concept ($\cong$2.9 to 3.2 m). A rotating RF joint is needed for the connection between the radar frontend and the antenna.

The slow rotation of the antenna translates to a faster scanning of the antenna footprint over the ocean surface than that of the fixed fan-beam concept. Thus, the number of pulse echoes falling over a given WVC is reduced, which needs to be compensated by increasing the number of range looks. Consequently, the range resolution, i.e., the system bandwidth, has to be increased proportionally to the necessary number of range looks. For maintaining the minimum SNR in the vicinity of 0 dB at the bottom of the dynamic range for a power-efficient design [12], the transmit power also needs to be increased. The net result is an increase of the radar dc power that is proportional to the antenna scan speed. As will be seen in Section V, a minimum scan speed of 2 r/min would be required for meeting the desired wind quality.

The design of the instrument is in principle simpler than that of the fixed fan-beam concept: it requires a single rotating antenna under the nadir face of the spacecraft, i.e., no switching matrix (replaced by an RF rotary joint) and no deployment in orbit. Nevertheless, the life expectancy and RF stability of the rotary joint may be an issue (although the total number of rotations is an order of magnitude lower than that of microwave imaging radiometers). Avoiding field-of-view conflicts with other instruments may be difficult in the case of multipayload mission. The overall predicted dc-power requirement (440 to 500 W) and data rate are higher than those of the fixed fan-beam concept, but the mass budget is lower (approximately 220 kg) due to the reduction in the number of antennas (six to one).

C. Rotating Pencil-Beam Concept

The rotating pencil-beam concept has heritage from the SeaWinds/QuickSCAT SCAs [4]. A pair of pencil beams,

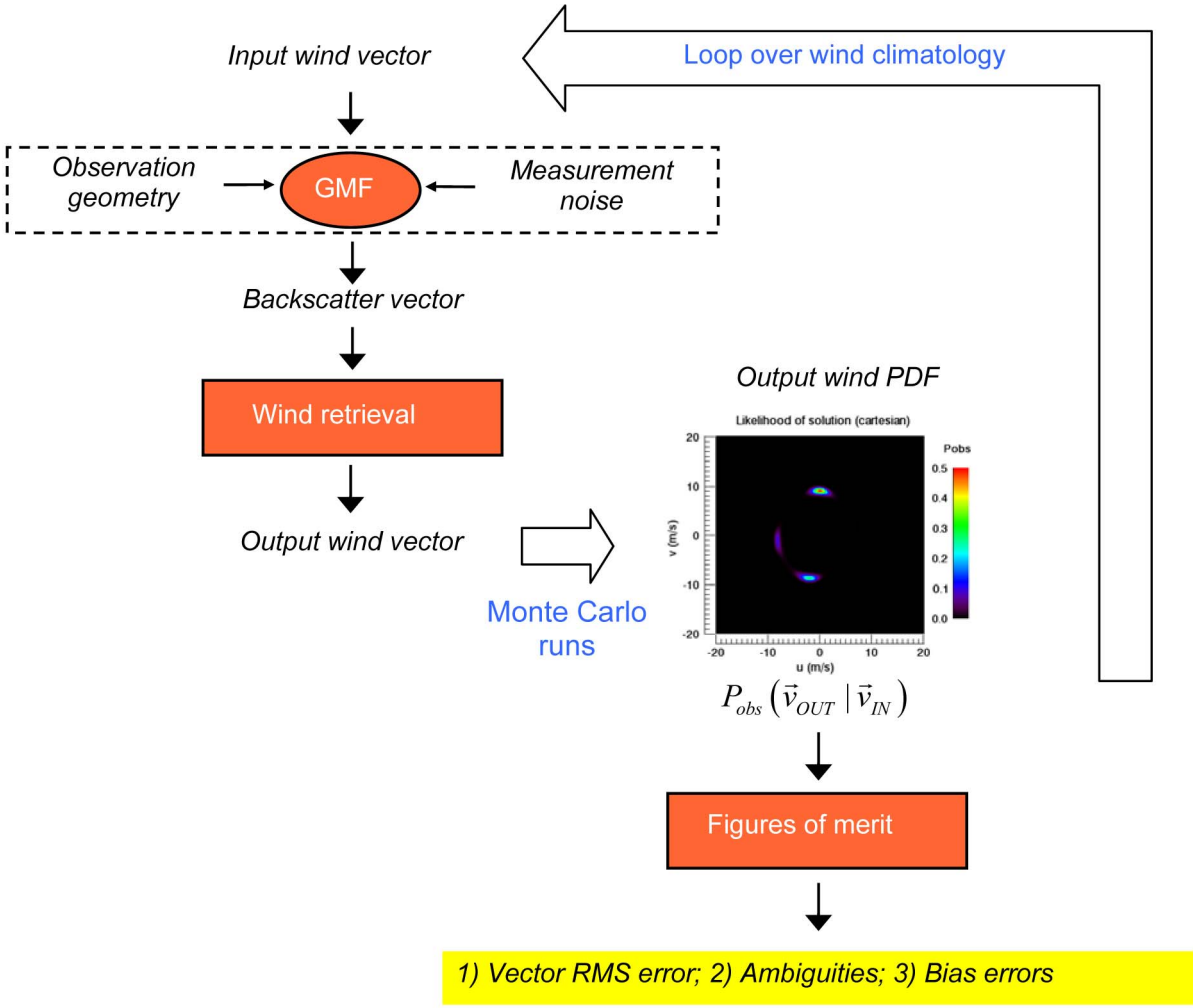

Fig. 4. End-to-end scatterometer performance assessment methodology.

respectively, pointed at two different incidence angles, is rotated around the nadir axis (conical scan) as shown in Fig. 3. Within the swath region covered by the inner beam, four azimuth views are acquired over each measurement cell, two forward and two backward, with azimuth angles dependent on the swath position. For WVCs lying outside the swath region covered by the inner beam (i.e., outer swath region), only two azimuth views are obtained. A full wind inversion, one that includes an estimation of the retrieved wind quality, is possible for those cells having four distinct azimuth views. The retrieval performance degrades around the subsatellite track due to reduced azimuth diversity in this part of the swath (i.e., azimuth views concentrating around 0° and 180°). In the outer swath region, the wind retrieval always results in ambiguous winds as will be shown in Section IV for simulated QuickSCAT data.

In the case of a real-aperture concept such as SeaWinds, the high rotation rate of the antenna (e.g., 18 r/min), necessary for achieving gapless coverage from one scan rotation to the next, results in a low number of along-scan looks. For example, for achieving the minimum radiometric resolution of 8% for the inner beam (incidence at 48°), more than 310 independent looks are required in total for a SNR of one [see (2)]. Thus, a high number of range looks would be required in order to compensate for the low number of along-scan looks. This would lead to a high system bandwidth, resulting in some significant transmit power requirement for meeting the optimum SNR, although the larger antenna aperture could somewhat counteract against the power increase. Taking into account of those design constraints, it is generally more difficult for this concept to meet the required radiometric resolution as exemplified by QuikSCAT with its significantly noisier data than those of ASCAT as seen in Fig. 9 (instrumental noise on the left). The estimated instrumental noise of QuickSCAT is approximately four times higher than that of ASCAT at equal resolution (50 km with 25 km sampling grid). Consequently, its number of looks should be increased by a factor of $4^2 = 16$ in order to meet the noise performance of ASCAT. For this comparison, the QuickSCAT pixels have been averaged with uniform weighting for achieving 50-km resolution, whereas ASCAT uses a Hamming Window weighting of the raw measurement samples.

Synthetic aperture radar (SAR) processing, combined with a high PRF, could substantially increase the number of along-scan looks. Such a concept was studied by NASA/JPL for

the QuickSCAT follow-on SCA mission [13]. The increased number of azimuth looks, when combined with the range looks, would allow for meeting the radiometric resolution requirement. Nevertheless, the high PRF and the necessary system bandwidth would result in high dc-power and high data rate, and SAR processing of the raw data would be required. Although, the SAR processing could be done on board the satellite, it would be complex due to the constantly changing Doppler-centroid of the radar echo as function of the beam position and further complicated by the antenna beam pointing uncertainties in real time. For ensuring the required radiometric performance, such processing should best be done on ground after Doppler-centroid estimation.

Finally, the major engineering hurdle of the rotating pencil-beam concept is the necessity of a large rotating antenna aperture. At C-band, the required aperture would have a diameter of 3 m (as compared to 1 m at Ku-band), rotating at a scan rate of approximately 18 r/min. Accommodation of a large aperture rotating antenna would cause considerable difficulties at the satellite level such as dynamic balancing of the rotating mass and provision of a free field-of-view around the antenna in case of multipayload platform. For example, the largest rotating reflector currently in orbit is that of Windsat with diameter of 1.8 m. In comparison to the rotating fan-beam concept, the life expectancy of the scan mechanism and RF stability of the rotating RF joint are aggravated by the much higher scan rate (QuickSCAT's designed life-time was 3 years, although it survived 10 years in orbit). Due to those high development risks, the rotating pencil-beam concept was discarded very early during the Phase 0 tradeoffs.

IV. End-to-End Performance Assessment Methodology

The SCA performance assessment methodology rests on the output wind statistics produced by an end-to-end SCA wind retrieval simulator, which is schematically shown in Fig. 4. The SCA wind retrieval simulator converts an input wind vector $(\mathbf{v}_{\mathrm{IN}})$ extracted from a world wind climatology [14] into a vector of error/noise-free backscatter coefficient measurements using the GMF sampled at observation angles specified by the SCA observation geometry. Measurement noise is then added to these backscatter coefficients according to the estimated system (instrumental + geophysical) noise levels and injected to the wind retrieval core of the simulator to generate an output wind vector $(\mathbf{v}_{\mathrm{OUT}})$. After a large number of wind inversions (or Monte Carlo runs), all the wind solutions are collected and binned into output wind probability density functions (PDFs) $P_{\mathrm{obs}}(\mathbf{v}_{\mathrm{OUT}}|\mathbf{v}_{\mathrm{IN}})$, which describe the statistical distribution of wind outputs for a particular wind input and allow the characterization of the retrieval error incurred by a particular SCA concept via mean statistics such as the wind vector root-mean-square (RMS) error, the wind vector bias or the presence of multiple ambiguous solutions. The climatologically averaged performance is then finally computed by repeating the above procedure over the wind climatology (see Fig. 5). The following sections describe in detail how these processes are implemented.

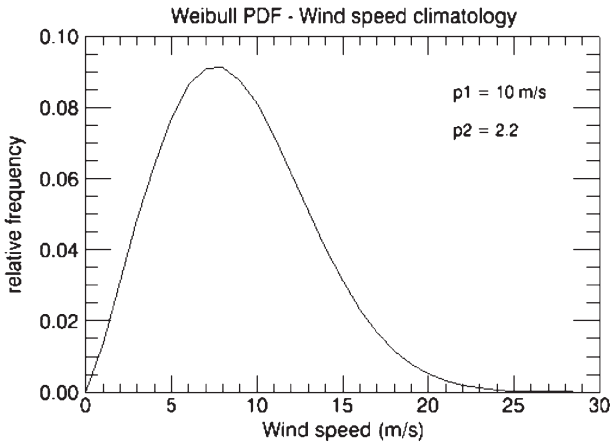

Fig. 5. Wind speed climatology (Weibull PDF [14]).

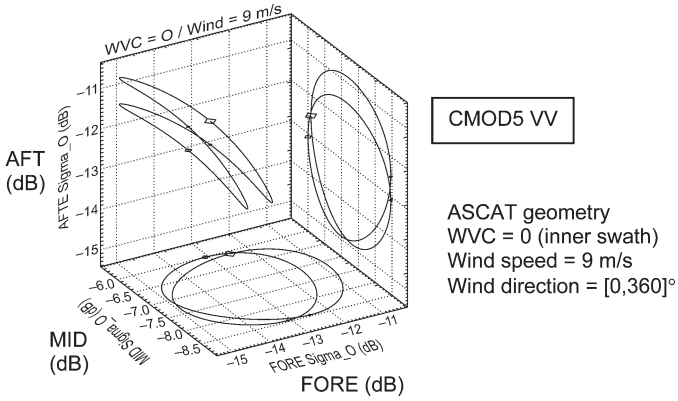

Fig. 6. CMOD5: C-band GMF in ASCAT measurement space (three views).

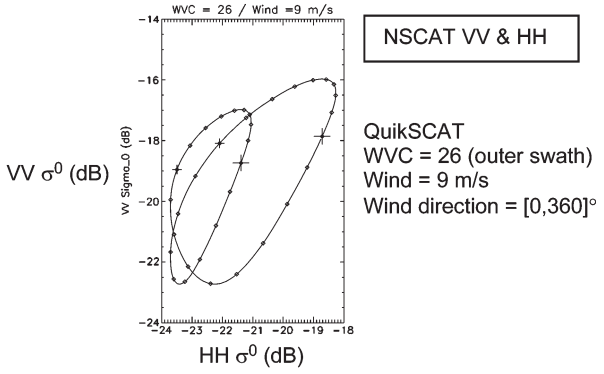

Fig. 7. NSCAT: Ku-band GMF in QuikSCAT measurement space (four views).

A. Input Wind

The retrieval of ocean wind vectors in scatterometry is a nonlinear problem and the error characteristics of the wind output depend on the wind input state. To eliminate this undesirable dependence on initial conditions, the SCA error characteristics are to be averaged over a world climatology of wind inputs characterized by a Weibull distribution in wind speeds [14], as given by (1), with a maximum around 8 m/s (see Fig. 5) and a uniform distribution in wind direction. It should however be

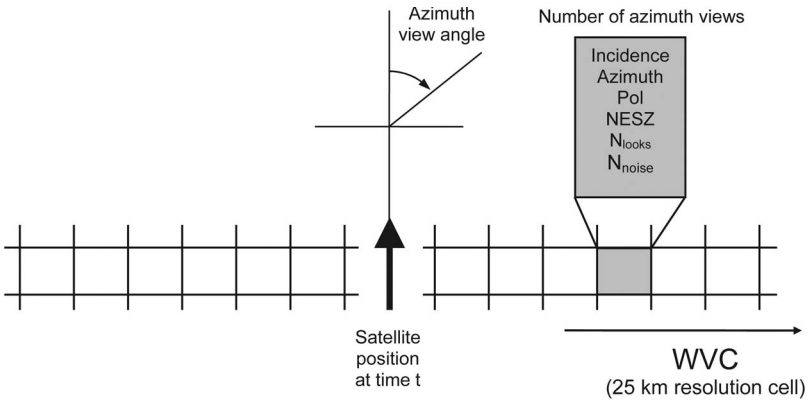

Fig. 8. Pseudo-level 1b product on a gridded swath.

noted that a world climatology of wind direction is not uniform due primarily to the trade winds

$$f(v) = \frac{p2}{p1}\left(\frac{v}{p1}\right)^{p2-1} e^{-\left(\frac{v}{p1}\right)^{p2}} \tag{1}$$

where $p1 = 10$ m/s and $p2 = 2.2$ m/s.

The input wind speeds are discretized from 3 to 16 m/s using steps of 1 m/s, covering about 90% of ocean wind states. The input wind directions are discretized from 0 to 360° using steps of 10°.

B. Geophysical Model Function

The GMF is an empirically derived function that relates backscatter measurements to surface wind vectors and viewing geometries in the form of $\sigma^0 =$ GMF (incidence angle, azimuth angle, wind vector). For C-band VV simulations, we use the CMOD5 model (see Fig. 6) for ocean backscatter [5], which is valid for incidence angles ranging from 18 to 58°. For Ku-band VV and HH retrieval simulations done below on QuickSCAT, we use the NSCAT backscatter numerical tables (see Fig. 7) [15].

C. Observation Geometry

The correct determination of the ocean wind vector signature requires that every WVC on the surface be visited by a number of azimuth views from a diversity of observation angles. A view consists of an incoherent average of independent looks as acquired by a beam over a given WVC. The observation geometry refers to the sequence of view angles (incidence and azimuth) at which the SCA beams intersect the surface, which is in general a function of the across-track distance of the WVC node, and of the beam rotation speed and timing for a rotating system. The observation geometry is calculated for every node on the swath using a simplified orbital model together with specific SCA instrument model parameters and stored as Pseudo-Level 1b products as shown in Fig. 8.

Other relevant information stored in Pseudo-Level 1b files are the transmitted polarization, the single look noise-equivalent-sigma-zero (NESZ) (NESZ $= \sigma^0/$SNR, also known as sensitivity), and the number of independent signal and noise looks $(N_{\text{looks}}, N_{\text{noise}})$ available per view. The NESZ describes the σ^0 level measured when the SNR is unity.

D. Measurement Noise

The system noise comprises both instrumental and geophysical components. The instrumental noise sets the system radiometric resolution, and it is modeled following [12] as

$$k_p^2 = \frac{\text{var}\{\sigma^0\}}{(\sigma^0)^2} = \frac{1}{N_{\text{looks}}}\left(1+\frac{1}{\text{SNR}}\right)^2 + \frac{1}{N_{\text{noise}}\text{SNR}^2} \tag{2}$$

where N_{looks} and N_{noise} refer to the number of independent signal and noise looks averaged per view, and SNR refers to the average SNR for a single look $(= \sigma^0/\text{NESZ})$.

The geophysical noise model is empirically adjusted to observed ASCAT and QuikSCAT noise behavior at 50-km resolution [6] and modeled as a function of wind speed as

$$\text{C-band} \quad k_{\text{geo}}(v) = 0.12\exp(-v/12) \tag{3}$$

$$\text{Ku-band} \quad k_{\text{geo}}(v) = 0.05 + 2.2 \cdot e^{-v/2} \tag{4}$$

which are valid for wind speeds of higher than about 2 to 3 m/s due to the limited sensitivity of those SCAs. The instrumental and geophysical noise contributions are assumed Gaussian and uncorrelated. For simulated observations, the total backscatter coefficient is modeled as

$$\sigma^0 = \sigma^0_{\text{GMF}}\left(1 + \sqrt{k_p^2 + k_g^2}\cdot N[0;1]\right) \tag{5}$$

where $N[0,1]$ is a Gaussian PDF with zero mean and unit standard deviation.

Fig. 9 displays typical levels of instrumental and geophysical noise observed by the QuikSCAT and ASCAT SCAs. ASCAT backscatter noise levels are consistent with the current 3-to-10% k_p requirement for the nominal mode (50-km resolution or 25-km gridding) at min/max backscatter conditions (i.e., low crosswind in outer swath and high upwind in inner swath).

E. Wind Retrieval

The retrieval of ocean winds from SCA data relies on the use of the GMFs, which relate the state variables, i.e., wind speed and wind direction, to backscatter measurements. The wind inversion is based on a search for minimum distances between backscatter measurements and backscatter model solutions lying on the empirical GMF surface. We define the normalized

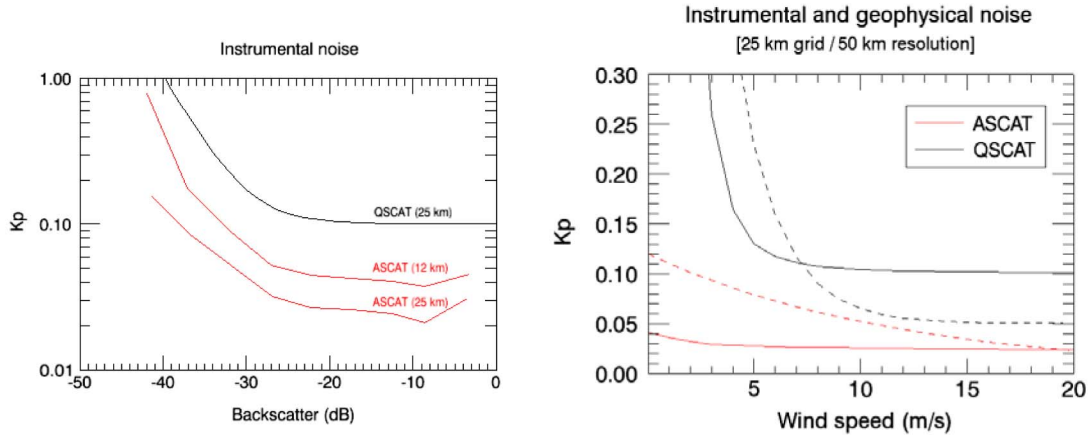

Fig. 9. Representative instrumental (continuous) and geophysical (dashed) noise levels at C- and Ku-band (instrumental noise as reported in KNMI/NOAA BUFR products).

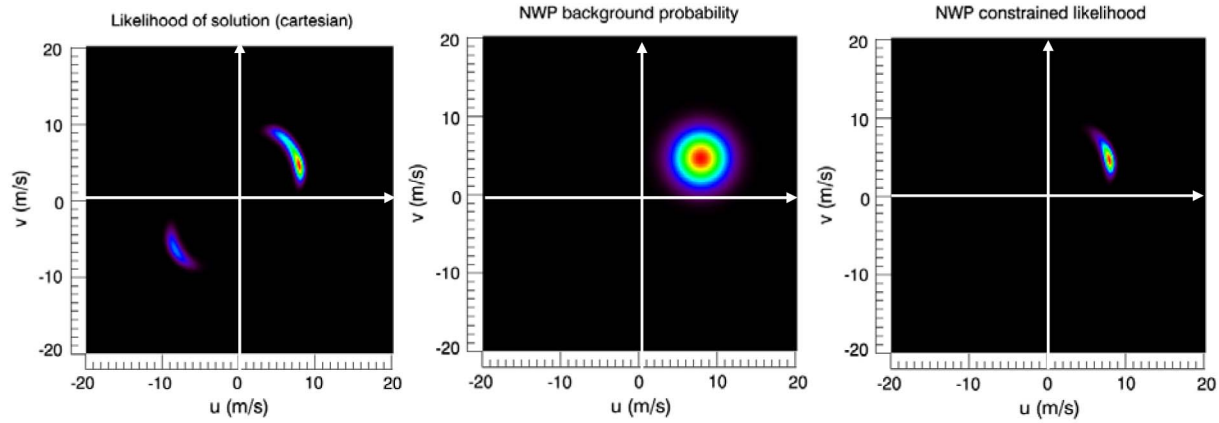

Fig. 10. Example of ambiguity removal in the end-to-end scatterometer performance model. Simulator output wind PDF (left); Gaussian NWP (background) probability (center); ambiguity-free output wind PDF (right) for QuikSCAT outer swath (WVC 26) with input wind 9 m/s at 30° and $k_p = 10\%$ with $\langle \text{MLE} \rangle = 5$.

square distance $\text{MLE}(\mathbf{v}|\sigma^0)$ from backscatter observations σ^0 to backscatter wind solutions $\sigma^0_{GMF}(\mathbf{v})$ on the GMF surface as

$$\text{MLE}(\vec{v}|\sigma^0) = \frac{1}{\langle \text{MLE} \rangle} \sum_{i=1\ldots N} \frac{\left|\sigma_i^0 - \sigma^0_{\text{GMF,i}}(\vec{v})\right|^2}{\text{var}\{\sigma_i^0\}} \quad (6)$$

where N is the dimension of the backscatter vector (i.e., the number of views per WVC node), $\text{var}\{\sigma^0\}$ is the instrumental noise variance and $\langle \text{MLE} \rangle$ is an empirical normalization factor that accounts for deviations from the ocean wind GMF due to geophysical noise, namely subcell wind variability and/or rain contamination. The normalized square distance MLE is but a sum of weighted square residuals between model and observed backscatter vectors, and the wind inversion consists of a search for minimum MLE across the space of solutions. The backscatter point on the GMF surface that lies the closest to observations yields the wind output, also known as the *first rank wind solution*.

Note that the SCA wind retrieval performance is affected by the presence of multiple ambiguous solutions, which arise from a combination of measurement noise, some nonideal observation geometries and proximity between the GMF up- and downwind branches. The process of selecting a wind solution among a set of likely candidates is called ambiguity removal, and the method used at KNMI (see, e.g., [16]) draws from numerical weather prediction (NWP) model information for this purpose. The problem is solved by minimizing a total cost function that combines both observational and NWP background contributions as

$$\begin{aligned} J =& -2\ln(\text{probability}) = J_{\text{obs}} + J_{\text{NWP}} \\ =& -2\ln\left(P_{\text{obs}}(\vec{v}|\vec{v}_0) \cdot P_{\text{NWP}}(\vec{v} - \vec{v}_{\text{NWP}})\right) \end{aligned} \quad (7)$$

which in terms of probabilities is equivalent to the product of the simulator output wind PDF $P_{\text{obs}}(\mathbf{v}|\mathbf{v}_0)$ for a given input wind $\mathbf{v}_0$ times a Gaussian probability distribution $P_{\text{NWP}}(\mathbf{v} - \mathbf{v}_{\text{NWP}})$ centered about a NWP "true" wind forecast $\mathbf{v}_{\text{NWP}}$ with a variance $\sigma^2_{\text{NWP}} \sim 5\ \text{m}^2/\text{s}^2$ in the wind components, resulting in an ambiguity-free output wind PDF $P_{\text{obs}}(\mathbf{v}|\mathbf{v}_0)P_{\text{NWP}}(\mathbf{v} - \mathbf{v}_{\text{NWP}})$. Fig. 10 illustrates an example of this ambiguity removal process applied on simulated QuickSCAT outer swath data which shows a 180° ambiguous wind. The NWP forecast variance σ_{NWP} has been chosen to be commensurate with the sum of the NWP model analysis and representativeness errors.

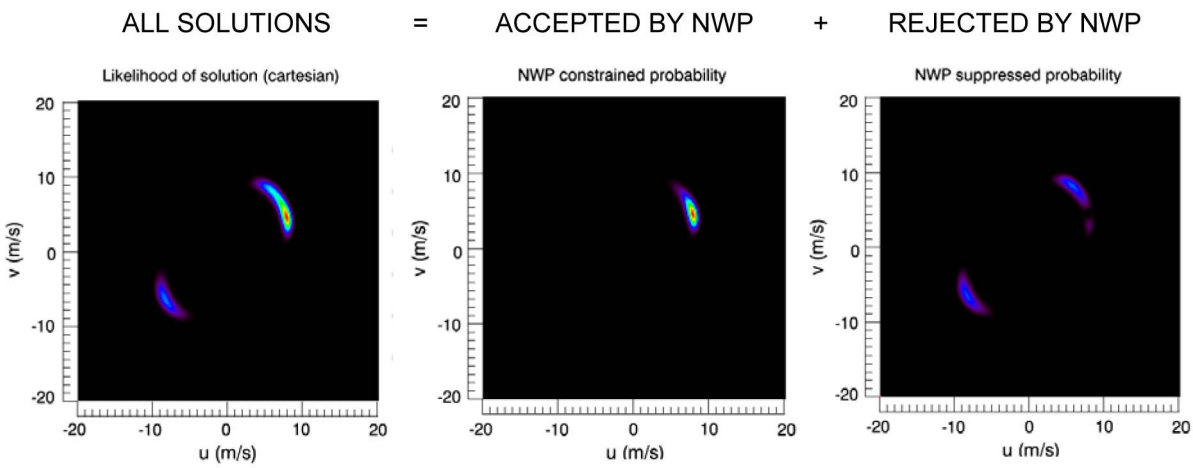

Fig. 11. (Left) Simulated output wind statistics $P_{\rm obs}(\mathbf{v}|\mathbf{v}_0)$. (Center) Filtered solutions after ambiguity removal $P_{\rm obs}(\mathbf{v}|\mathbf{v}_0)P_{\rm NWP}(\mathbf{v}-\mathbf{v}_{\rm NWP})$. (Right) NWP suppressed solutions $P_{\rm obs}(\mathbf{v}|\mathbf{v}_0)(P_{\rm NWP,max}-P_{\rm NWP}(\mathbf{v}-\mathbf{v}_{\rm NWP})$, for QuikSCAT outer swath (WVC 26) with input wind 9 m/s at 30° and $k_p = 10\%$ with $\langle \text{MLE} \rangle = 5$.

Figure of Merit (1): Wind Vector RMS Error

At NWP centers, the quality of a wind measurement is usually referred to a vector RMS error. Along this line, our first Figure of Merit (FoM) is defined as the wind vector RMS error calculated from the ambiguity-free output wind PDF defined in the previous section and normalized by the NWP background uncertainty as

$$\text{FoM}_{\rm VRMS} = \frac{\text{RMS}_{\rm obs}}{\text{RMS}_{\rm NWP}} \subset [0,1] \tag{8}$$

where

$$\text{RMS}_{\rm obs} = \left(\int |\vec{v}-\vec{v}_{\rm true}|^2 P_{\rm obs}(\vec{v}|\vec{v}_{\rm true}) \times P_{\rm NWP}(\vec{v}-\vec{v}_{\rm true}) d^2v \right)^{1/2}$$

$$\text{RMS}_{\rm NWP} = \left(\int |\vec{v}-\vec{v}_{\rm true}|^2 P_{\rm NWP}(\vec{v}-\vec{v}_{\rm true}) d^2v \right)^{1/2} = \sqrt{2}\sigma_{\rm NWP} \tag{9}$$

and $\sigma_{\rm NWP} = \sqrt{5}$ m/s is the NWP background uncertainty standard deviation. The simulator output wind PDF, $P_{\rm obs}(\mathbf{v}|\mathbf{v}_{\rm true})$, represents the statistical frequency of output solutions given a particular wind input, or number of wind vector solutions that fall in the interval $(u, u+du)$ and $(v, v+dv)$ divided by the total number of trials conducted in the Monte Carlo simulation. The output wind PDF is scaled by a constant to guarantee that the integral under $P_{\rm obs} \times P_{\rm NWP}$ is unity, and

$$P_{\rm NWP}(\vec{v}-\vec{v}_{\rm true}) = \frac{1}{2\pi\sigma^2_{\rm NWP}} \exp\left(|\vec{v}-\vec{v}_{\rm true}|2/(2\sigma^2_{\rm NWP})\right). \tag{10}$$

This FoM quantifies the relative standard deviation of simulated output wind solutions about the true wind with respect to the background error after NWP-based ambiguity removal, and it should be as low as possible.

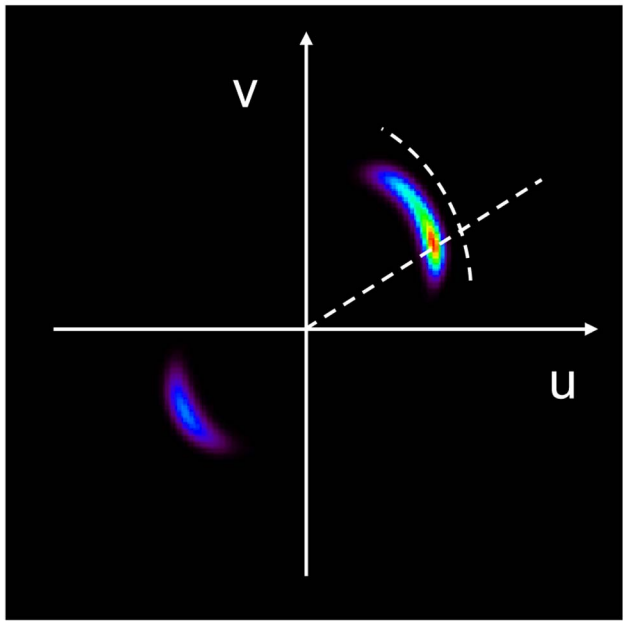

Fig. 12. Skewed output wind statistics give way to systematic biases in wind speed and most notably, in wind direction. In this example, the true wind lies at 9 m/s at 30°, but the wind outputs are drawn to a 45° solution (QuikSCAT, WVC = 26).

Figure of Merit (2): Ambiguity Susceptibility

Another performance figure should quantify the ability of a SCA to handle ambiguous solutions or function without a priori NWP model information. Our next FoM is defined as the fraction of solutions that are rejected by the NWP background constraint, defined as $P_{\rm obs}(P_{\rm NWP,max} - P_{\rm NWP})$, relative to the number of solutions accepted by the NWP background constraint, defined as $P_{\rm obs}P_{\rm NWP}$, and expressed as

$$\text{FoM}_{\rm AMBI} = P_{\rm NWP,max} \int P_{\rm obs}(\vec{v}|\vec{v}_{\rm true}) d^2v - 1 \subset [0,\infty]. \tag{11}$$

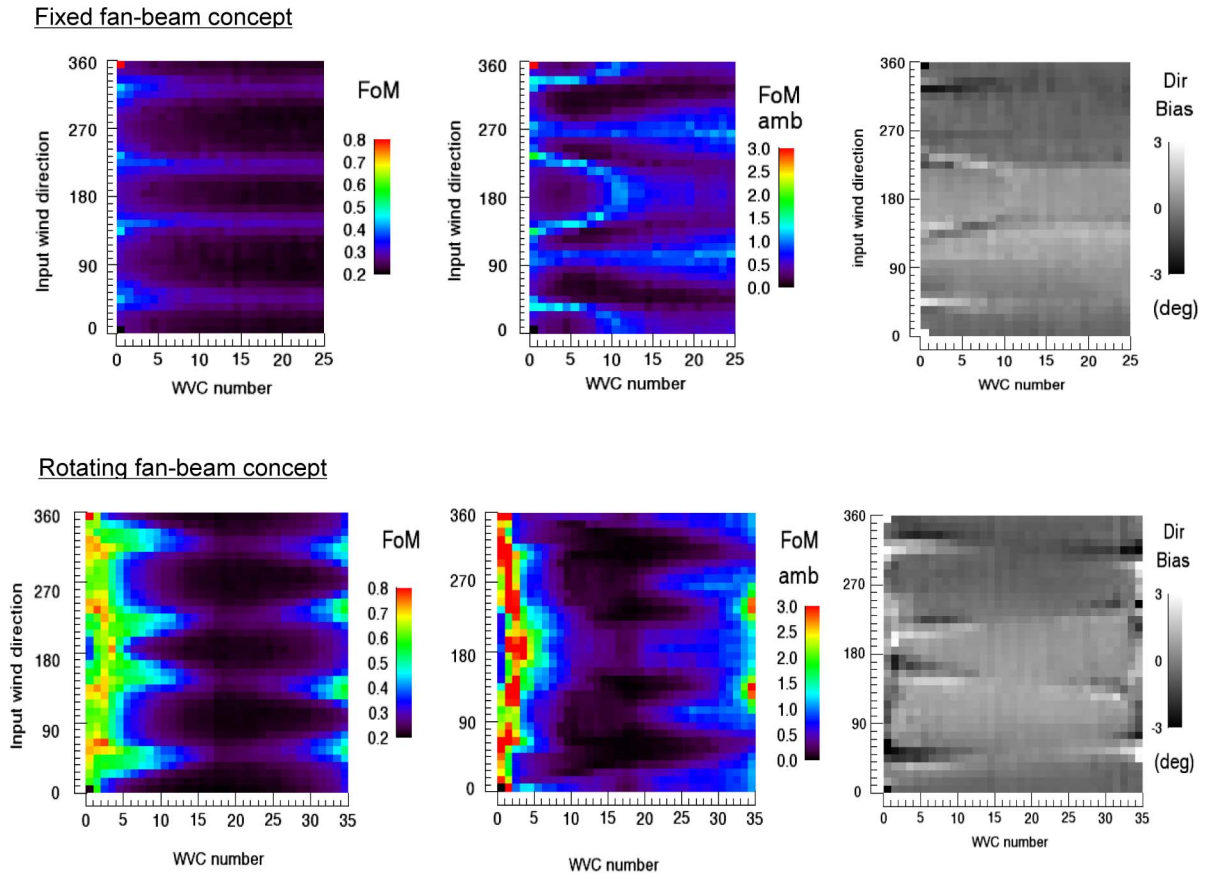

Fig. 13. (Top row) Fixed fan-beam and (bottom) rotating fan-beam (2 r/min) FoMs as a function of across-track location and wind direction (wind speed is 9 m/s). Wind direction is measured clockwise from the axis of abscissas in across-track direction pointing toward east. The WVC numbers increase with stand-off distance from the subsatellite track.

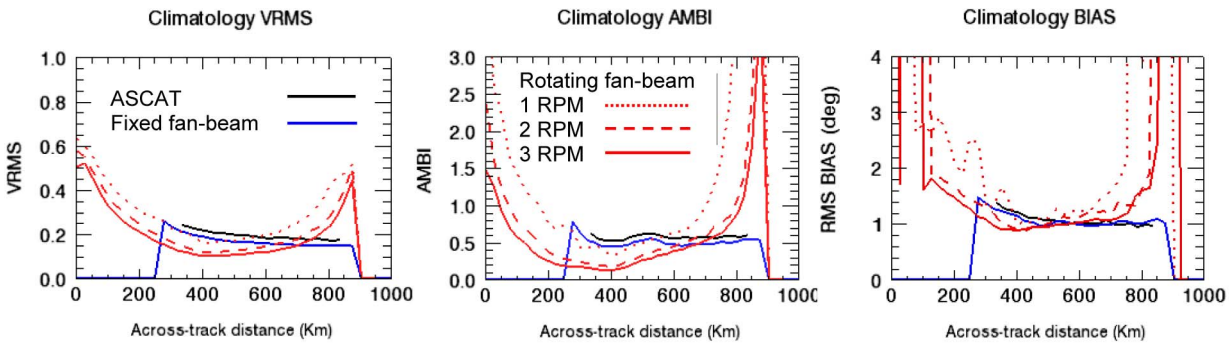

Fig. 14. Average climatology wind (3–16 m/s and uniformly directional distribution) FoMs for (blue) fixed fan-beam concept and (red) rotating fan-beam concept as a function of across-track distance. ASCAT performance on *MetOp* is shown in black for reference.

In Fig. 11, the simulated QuickSCAT data as example of ambiguity removal (Fig. 10) are again used in order to illustrate the different probability terms contributing to (11). This FoM quantifies the significance of the NWP background information for SCA wind retrieval (i.e., ambiguity removal), and it should be as low as possible.

Figure of Merit (3): Bias Errors

Bias errors arise from degrees of asymmetry (or skewness) in the output wind PDFs, which cause the mean of the distribution (or average location of the output wind solution) to be shifted from the distribution mode (or location of the true wind, see Fig. 12 for example of the simulated QuickSCAT data). Systematic vector wind biases can be calculated as

$$\overrightarrow{\text{bias}} = \langle \vec{v} \rangle - \vec{v}_{\text{true}} = \int (\vec{v} - \vec{v}_{\text{true}}) \cdot P_{\text{obs}}(\vec{v}|\vec{v}_{\text{true}}) P_{\text{NWP}}(\vec{v} - \vec{v}_{\text{true}}) d^2 v. \quad (12)$$

Because systematic errors along the wind radial direction (output wind speed biases) are small in general, we will not

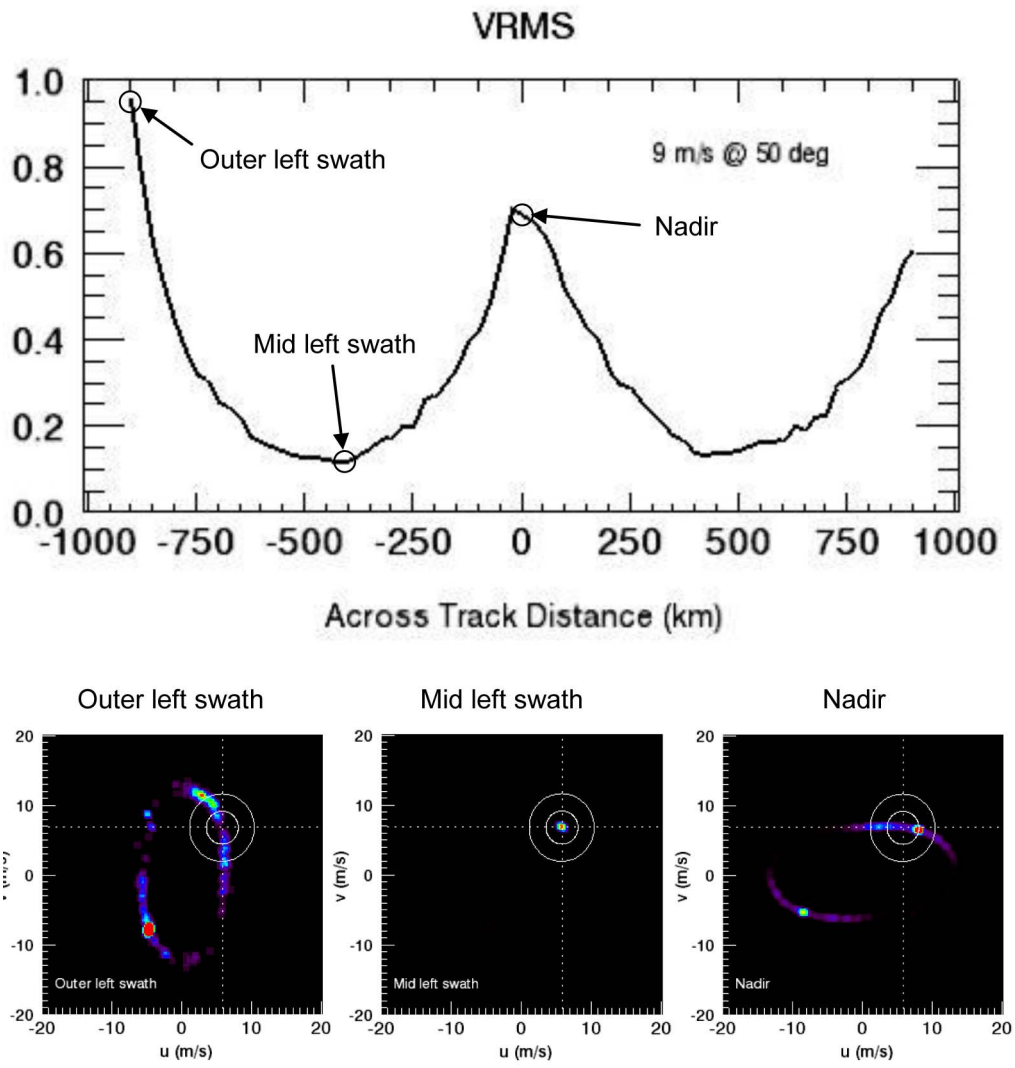

Fig. 15. (Upper) Vector RMS error and (lower) wind PDF for the rotating fan-beam concept with a scan speed of 2 r/min. The input wind is 9 m/s at 50°. The concentric rings represent the background wind probability density at respectively one and two standard deviations.

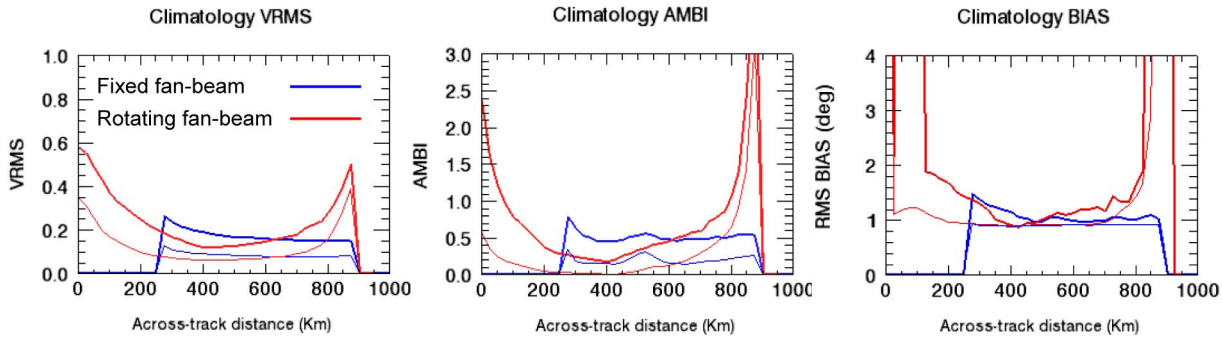

Fig. 16. Average climatology wind (3–16 m/s and uniform directional distribution) FoMs for (blue) fixed fan-beam concept and (red) rotating fan-beam concept (2 r/min) as a function of across-track distance with (thick line) and without (thin line) geophysical noise.

consider them further. However, the presence of systematic errors along the wind azimuth direction (output wind direction biases) produces artificial directional preferences that may corrupt the observed wind climatology.

V. Wind Retrieval Performance

Figs. 13 and 14 summarize the performance figures for the fixed fan-beam and rotating fan-beam concepts using instrumental noise levels that comply with the technical requirements

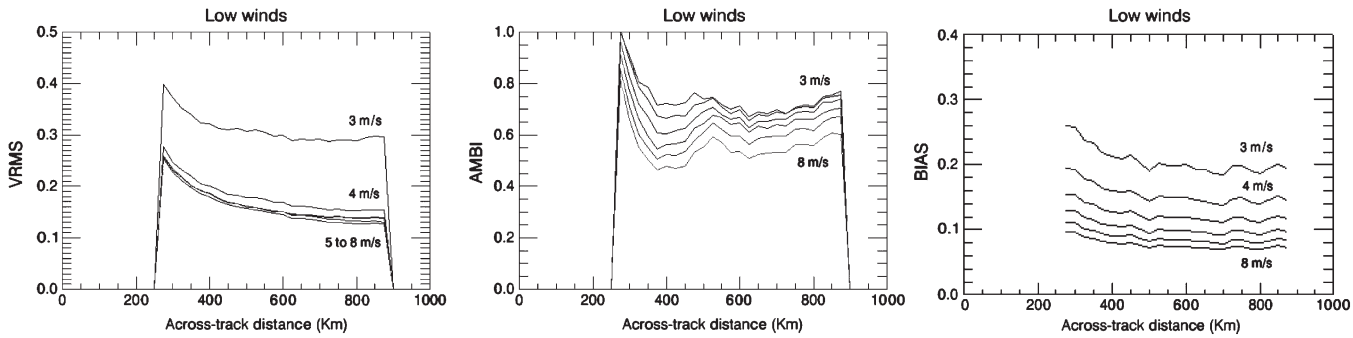

Fig. 17. Low wind FoMs ($\leq$ 8 m/s) for the fixed fan-beam (baseline) concept as a function of across-track distance.

and geophysical noise levels given by (3). No such performance assessment was made for the rotating pencil-beam concept which was discarded for reasons explained in Section III. Fig. 13 shows the three FoM as function of across-track nodal position and wind direction for 9 m/s wind, as their directional dependence appears most pronounced at this particular wind speed. It is recalled that the first FoM is normalized to the NWP background uncertainty of $\mathrm{RMS}_{\mathrm{NWP}} = \sqrt{10}$ m/s. The upper pictures give results for the fixed fan-beam concept and the lower pictures for the rotating fan-beam concept with an antenna scan speed of 2 r/min. Fig. 14 shows a more condensed result as a function of the across-track position only. Here, the FoMs have been averaged over all wind directions and a climatology of wind speeds discretised from 3 to 16 m/s with steps of 1 m/s. For the rotating concept, three different scan speeds have been considered in this performance estimation (1, 2, and 3 r/min).

The FoM scores indicate that the wind quality of the fixed fan-beam concept remains quite uniform across the swath (Fig. 13—upper). There is slight performance degradation at a number of distinct zones in wind direction, which reflects the particular measurement geometry of this concept and properties of the GMF. The retrieval performance also degrades slightly toward the low incidence end of the swath, which was actually expected due to the relaxation of the radiometric resolution requirement below incidence of $25^{\circ}(k_p \leq 3\%)$. As a matter of fact, this relaxation was introduced in order to limit the radar power to a reasonable level.

The performance of the rotating fan-beam concept (Fig. 13—lower) depends strongly on across-track location and degrades significantly at nadir and swath edges as anticipated. Similar to the case of the fixed fan-beam concept, there is also a slight performance modulation as a function of the wind direction. The performance of this concept depends strongly on the antenna rotation speed as seen in Fig. 14 (red curves). In any case, the extent of the comparably useful swath remains similar for both the fixed and rotating fan-beam concepts and is limited to about 650 km per side for a wind vector RMS error of $\leq$ 0.6 m/s if the antenna scan rate of the latter is $\geq$ 2 r/min. A definite strength of the rotating fan-beam concept lies in its very low ambiguity scores (low dependability on NWP background support for ambiguity removal) over the extent of its usable swath. The generally higher number of azimuth views in the usable parts of the swath seems to contribute to this trend. Another attractive feature of this concept is that the RMS error

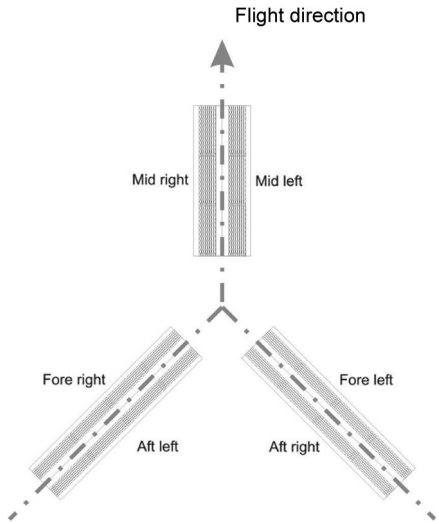

Fig. 18. SCA antenna configuration. Mid-antenna assembly is 2.9 to 3.2 m long; Fore- and aft-antenna assemblies are 3.6 to 4 m long.

does not exceed 2 m/s in the nadir region. The usefulness of retrieved wind from this region for NWP applications needs to be assessed by dedicated impact experiments. Nevertheless, the concept offers a better synoptic view of large-scale storm events and better synergy with other companion payloads such as passive microwave imager that have observations centered on nadir.

Fig. 15 shows specific examples of retrieval simulations for the rotating fan-beam concept with a scan speed of 2 r/min. The upper picture shows the vector RMS error for a wind of 9 m/s at 50° over the complete swath (1800 km), and the lower pictures the retrieved wind PDF at three different swath locations. The concentric rings in the lower pictures indicate the Gaussian background wind probability density, respectively, at one and two standard deviations around the true wind. The worst case result is seen at the left edge of the swath where a 180° ambiguous wind (9 m/s at 230°) dominates against the true wind. At midswath between the left edge and nadir, no ambiguity is observed which explains the robustness of this concept against wind ambiguity. At nadir, a small directional bias of the nominal solution is observed together with a weak 180° ambiguity.

To gain an appreciation on how geophysical noise affects the SCA performance figures, Fig. 16 shows the FoMs with

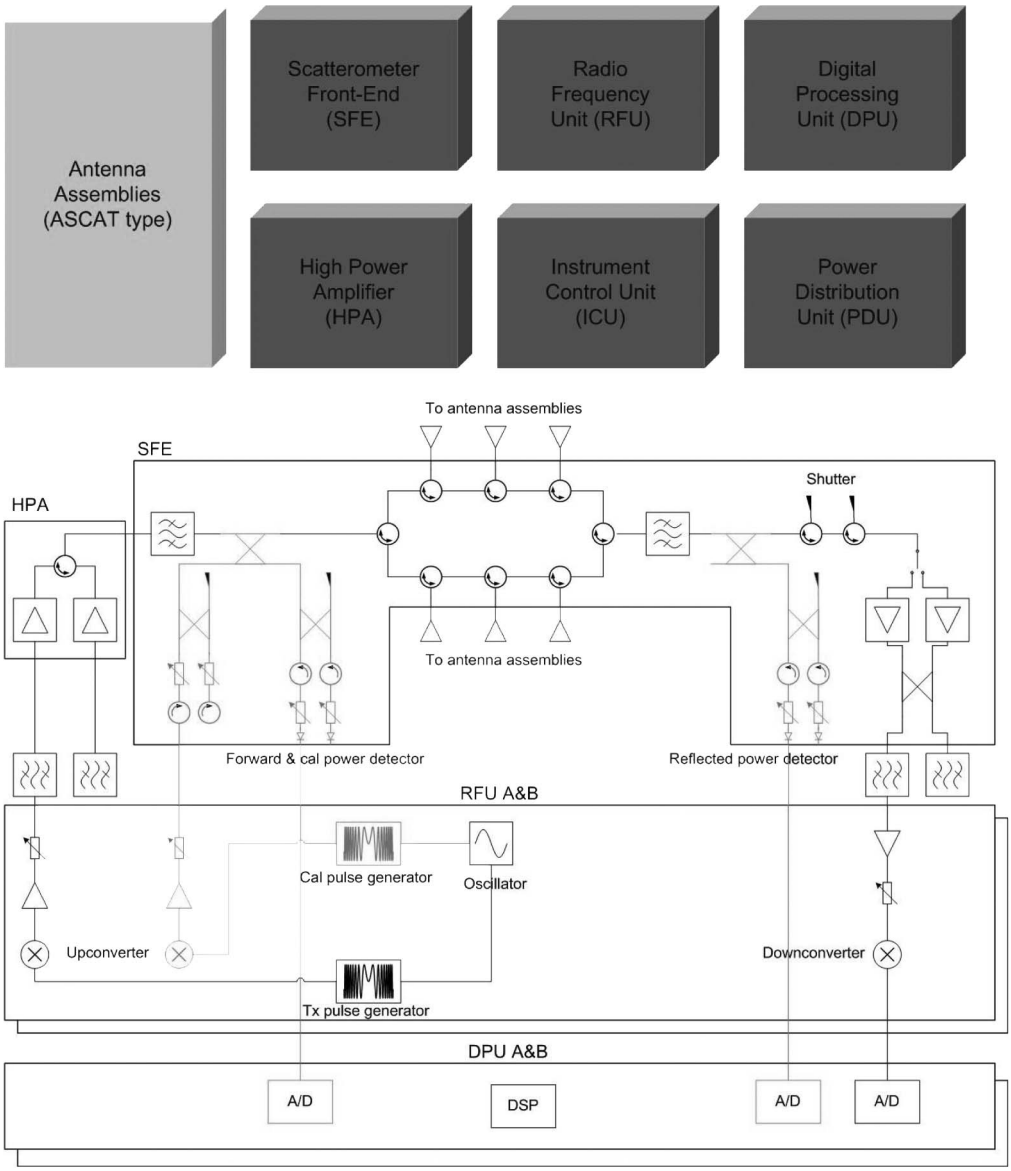

Fig. 19. (Upper) SCA instrument block diagram and (Lower) details of the front-end (SFE), high power amplifier (HPA) and radio frequency unit (RFU).

and without geophysical noise for the two concepts. One can observe that the geophysical noise contribution accounts for about a half of the simulated wind vector RMS error (left most picture), whereas the ambiguity susceptibility increases significantly (central picture). The impact of geophysical noise on wind bias appears to be low, as the former is uniform over all wind direction.

Finally, Fig. 17 shows the performance of the fixed fan-beam concept for wind speeds below 8 m/s. It can be seen that the vector RMS error remains below 1.3 m/s for 3 m/s wind.

VI. Selection of Baseline and Preliminary Instrument Design

The fixed fan-beam concept with six antennas has been selected as baseline at the end of Phase 0 primarily on the grounds of maintaining continuity of the operational ASCAT observations and maturity of the associated level 2 data processing algorithms. The yet unknown technological risks associated with the rotating fan-beam concept were perceived as a weakness in the preparation of the EPS-SG development program. The slight performance advantages as predicted by the end-to-end simulation analysis of the new concept were not considered to outweigh the proven ASCAT-type concept for NWP applications.

The observation swaths of the baseline concept extend from 260 km to 900 km stand-off distances on both sides of the subsatellite track. The antenna configuration (for the baseline VV polarization only) is shown in Fig. 18, which consists of three pairs of planar arrays arranged in an inversed Y-configuration, to be accommodated on the nadir face of the spacecraft. The antenna dimensions, particularly in the length direction, are constrained by the available platform space and vary in the range of 2.9 to 3.2 m for the mid-antennas and 3.6 to 4 m for the fore- and aft-antennas. Fore- and aft-antenna assemblies shall be stowed for launch and deployed in orbit. The three antenna assemblies can be configured differently if necessary for accommodation reasons, provided that the

TABLE II
SCA DESIGN PARAMETERS

Parameter	Mid-Beam	Fore-/Aft-Beam
Orbit	817 km	
PRF (for 6 beams)	185 Hz	175 Hz
Peak RF power	580 W	
Pulse length	0.56 ms	
Incidence at near swath edge	20°	27.4°
Incidence at far swath edge	53.5°	64.7°
Data rate	4 Mbits/s	
Mass	360 - 500 kg	
DC-power	430 - 530 W	

respective orientation in azimuth is maintained. The antennas consist of slotted waveguide arrays, made of aluminum or metallized carbon-fiber reinforced plastic (CFRP) subject to further tradeoffs for meeting the stringent radiometric stability requirement. They are connected through waveguides to the beam-switching matrix. For the fore-/aft-antenna assemblies, rotating RF joints are required for enabling deployment. Each of the antenna assemblies is mounted on a CFRP support structure for ensuring a very high pointing stability.

The instrument block diagram is shown in Fig. 19 (upper) together with details of the front-end (SFE), high power amplifier (HPA), and radio frequency unit (RFU) in the lower part. The baseband radar pulse is stored in the digital memory read-out and followed by the digital-to-analog converter. The analog pulse is then upconverted to the carrier frequency by a quadrature mixer. The tradeoff between the nonmodulated and modulated transmit pulse is still ongoing, and this will have impacts on the radar PRF and peak power necessary from the HPA. The HPA consists of a traveling wave tube or a klystron driven by a high voltage electronics power conditioner. The HPA feeds the six antennas sequentially through the beam-switching matrix.

The receive signal is amplified by the low noise amplifier (LNA) and downconverted to the in-phase (I) and quadrature phase (Q) baseband signals (not explicitly shown). The digitized I and Q baseband signals could be detected and multilooked on board (incoherent summation of the detected echo profiles). In the case of modulated pulse concept, the I and Q signals are first pulse compressed before detection. Alternatively, the digitized I and Q signals could be downlinked and further processed on ground. The later option would substantially increase the data amount to be downlinked with corresponding system impacts. The HPA and RFUs are fully redundant, whereas the front-end has only internally redundant LNAs.

An internal calibration loop measures the transmit pulses at the output of the HPA and that of the beam-switching matrix. The calibration pulses are also injected at the input of the beam-switching matrix and measured at the input of the LNA. Those measurements enable gain characterization of the transmit and receive chains, as well as losses of the components in the radar front-end. The necessity of measuring the pulses or injecting calibration pulses at the input ports of the antennas is a subject of further analysis in relation to meeting the radiometric stability requirement.

The instrument also measures the thermal noise in the absence of radar echo for determining the background noise level. After the noise estimation on ground, noise substraction is performed for determining the unbiased ocean surface radar cross section.

In the ground processing, 2-D Hamming window function is applied over the WVC nodes for averaging the detected raw samples (multilooking) and for optimizing the level 1 product spatial resolution.

Table II summarizes the major design parameters. The use of a short, chirp-modulated transmit pulse was assumed for the design optimization. The optimization of the pulse length, taking into account the feasibility of the HPA, is a subject of tradeoffs in Phase A, and this will have an impact on the peak RF power. Instrument mass and dc-power estimates at the end of Phase 0 depend on the selected antenna dimensions (2.9 to 3.2 m for mid- and 3.6 to 4 m for fore-aft) and vary respectively in the range of 360 to 500 kg and 530 to 430 W with increasing antenna length for the baseline (VV) concept. Implementation of the HH or VH polarization on a subset of beams, in addition to the VV-polarization on all beams, is a subject of further tradeoffs.

VII. CONCLUSION

A fixed fan-beam SCA concept, similar to the *MetOp*'s ASCAT instrument, has been selected as baseline for the EPS-SG mission at the end of Phase 0 primarily on the grounds of maintaining measurement continuity. The tradeoffs during Phase 0 considered three distinct instrument concepts, out of which the fixed fan-beam and rotating fan-beam concepts were compared in more detail in terms of engineering design and end-to-end wind retrieval performance. A uniform and objective methodology for the performance assessment of dissimilar SCA concepts has been developed. The performance model rests on statistics produced by an end-to-end SCA wind retrieval simulator run in a Monte Carlo fashion. Three FoMs have been proposed as a means to examine the different aspects that affect the quality of SCA wind products: 1) the wind vector RMS error; 2) the susceptibility to ambiguities, and; 3) the presence of biases. The performance model results reveal and quantify the inherent capabilities of different SCA configurations under realistic instrumental and geophysical noise conditions. The performance model results indicate that the wind retrieval performance of the fixed fan-beam concept is rather uniform across the swath, while that of rotating fan-beam concept remains strongly dependent on across-track location, degrading at nadir and at the swath edges as expected due to the reduced azimuth diversity in those parts of the swath. Nevertheless, the performance of the latter is comparable to or slightly better than that of the former in terms of FoMs and usable swath extensions. Therefore, both concepts can meet the observation requirements of the EPS-SG mission, with some advantages for the rotating fan-beam concept in terms of: 1) robustness against wind directional ambiguities, allowing it to rely less on the accuracy of the background wind field; 2) gapless coverage in the nadir region with a vector RMS error of less than 2 m/s. However, these slight performance advantages

of the new concept were not considered to outweigh the proven ASCAT-type concept for NWP applications. It is nevertheless worth noting that a Ku-band rotating fan-beam SCA is under development for the Chinese French Ocean Satellite for launch in 2014 [17]. Works on the selected baseline during the upcoming EPS-SG Phase A will include further refinements in instrument design definition and corresponding performance sensitivity studies. This will also include investigation of feasibility for adding a HH or VH polarization capability in conjunction with an assessment of its usefulness at high wind speeds and the refinement of the SCA geophysical noise models.

ACKNOWLEDGMENT

The authors would like to acknowledge the excellent instrument engineering work done by the two industrial teams for the definition of EPS-SG SCA: Astrium-GmbH, Germany and Thales Alenia Space Italy.

REFERENCES

[1] M. Betto, C. Accadia, S. Banfi, P. Bensi, J.-L. Bézy, V. Kangas, S. Kraft, C. C. Lin, R. Meynart, P. Phillips, L. Sarlo, P. Silvestrin, P. Schluessel, and J. Wilson, "Post-EPS system concept," in *Proc. EUMETSAT Meteorol. Satellite Conf.*, Bath, U.K., Sep. 21–25, 2009.

[2] S. Banfi, P. Schlüssel, C. Keegan, M. Betto, C. C. Lin, V. Kangas, S. Kraft, P. Bensi, I. Zerfowski, M. Saccoccio, and T. Maciaszek, "Feasibility studies for the follow-on EUMETSAT polar system," in *Proc. SPIE Remote Sens. Eur. Int. Symp.*, Toulouse, France, Sep. 2010, p. 78 260.

[3] C. C. Lin, J. Wilson, F. Impagnatiello, and P. S. Park, "An analysis of a rotating, range-gated, fanbeam spaceborne scatterometer concept," *IEEE Trans. Geosci. Remote Sens.*, vol. 38, no. 5, pp. 2114–2121, Sep. 2000.

[4] M. W. Spencer, C. Wu, and D. G. Long, "Improved resolution backscatter measurements with the SeaWinds pencil-beam scatterometer," *IEEE Trans. Geosci. Remote Sens.*, vol. 38, no. 1, pp. 89–104, Jan. 2000.

[5] A. Verhoef, M. Portabella, A. Stoffelen, and H. Hersbach, CMOD5.n—The CMOD5 GMF for Neutral Winds, OSI SAF Report, SAF/OSI/CDOP/KNMI/TEC/TN/165, 2008. [Online]. Available: http://www.knmi.nl/scatterometer/publications/

[6] M. Portabella and A. Stoffelen, "Scatterometer backscatter uncertainty due to wind variability," *IEEE Trans. Geosci. Remote Sens.*, vol. 44, no. 11, pp. 3356–3362, Nov. 2006.

[7] Post-EPS Mission Requirements Document, EUMETSAT Document No. EUM/PEPS/REQ/06/0043, Damstadt, Germany, Jun. 25, 2010. [Online]. Available: http://www.eumetsat.int/groups/pps/documents/document/pdf_peps_mrd.pdf

[8] J. Sapp, J. Dvorsky, S. J. Frasier, P. Chang, Z. Jelenak, and T. Hartley, "High-wind dual-polarization NRCS measurements at C- and Ku-band during Winter 2011," in *Proc. IOVWST Meeting*, Annapolis, MD, May 2011.

[9] P. W. Vachon and J. Wolfe, "C-band cross-polarization wind speed retrieval," *IEEE Geosci. Remote Sens. Lett.*, vol. 8, no. 3, pp. 456–459, May 2011.

[10] C. C. Lin, J. Wilson, F. Impagnatiello, and P. S. Park, "Rotating, range-gated fanbeam imaging radar: A new spaceborne scatterometer concept," in *Proc. PIERS Workshop Adv. Radar Methods*, Baveno, Italy, Jul. 1998.

[11] C. C. Lin, A. Stoffelen, J. de Kloe, V. Wismann, S. Bartha, and H.-R. Schulte, "Wind retrieval capability of rotating, range-gated, fanbeam spaceborne scatterometer," in *Proc. SPIE Int. Symp. Remote Sens.*, Crete, Greece, Sep. 23–27, 2002, p. 268.

[12] R. E. Fischer, "Standard deviation of scatterometer measurements from space," *IEEE Trans. Geosci. Electron.*, vol. GE-10, no. 2, pp. 106–113, Apr. 1972.

[13] R. W. Gaston and E. Rodriquez, "QuikSCAT Follow-on Concept Study, JPL Publication 08-18," Jet Propulsion Laboratory, Pasadena, CA, Apr. 2008.

[14] W. T. Liu, W. Tang, and X. Xie, "Wind power distribution over the ocean," *Geophys. Res. Lett.*, vol. 35, p. L13 808, Jul. 2008.

[15] F. J. Wentz and D. K. Smith, "A model function for the ocean-normalized radar cross section at 14 GHz derived from NSCAT observations," *J. Geophys. Res.*, vol. 104, no. C5, pp. 11 499–11 514, 1999.

[16] J. Vogelzang, "Two dimensional variational ambiguity removal (2DVAR)," EUMETSAT, Darmstadt, Germany, Tech. Rep. NWPSAF-KN-TR-004, 2007.

[17] X. Dong, W. Lin, and D. Zhu, "System description and performance of the scatterometer of CFOSat satellite," in *Proc. EUMETSAT/ESA Scatterometer Sci. Conf.*, Darmstadt, Germany, Apr. 2011.

Chung-Chi Lin was born on November 8, 1952, in Kokura City, Japan. He received the Diploma degree from the Swiss Federal Institute of Technology, Lausanne, Switzerland, in 1979 and the M.S. and Ph.D. degrees from the University of California, Berkeley, in 1982 and 1985, respectively, all in electrical engineering.

From 1979 to 1980, he was a scientific collaborator at the High Voltage Laboratory of the Swiss Federal Institute of Technology, Lausanne, working in the area of electromagnetic compatibility and nuclear electromagnetic pulse protection. From 1980 to 1985, he was a Research Assistant at the Electronics Research Laboratory of the University of California, Berkeley, in the field of numerical methods for electromagnetics. From 1985 to 1993, he worked at Dornier System (currently EADS-Astrium GmbH) in Friedrichshafen, Germany, in the areas of satellite (ERS-1), automotive and ground-based radars, planar antennas, and high-temperature superconducting microwave circuits. In 1993, he joined the European Space Technology Centre of ESA in Noordwijk, The Netherlands. His area of responsibility is development of microwave payloads for future Earth Observation missions. Since 2000, he has been the Head of Microwave Instruments Section in the Earth Observation Programs. Lately, he has been contributing to the new cycle of Earth Explorer candidate mission preparation (7th Earth Explorer) and the next-generation low Earth orbiting meteorological satellite system payloads (*MetOp* Second Generation). His recent interests are orbital radars for subsurface sounding.

Dr. Lin was the Guest Editor of the PROCEEDINGS OF THE IEEE special issue on Solar System Radar & Radio Science (May 2011).

Maurizio Betto received the M.S. degree in astronomy from University Padua, Padua, Italy, in 1988 and the Ph.D. degree in electrical engineering from the Technical University of Denmark, Lyngby, Denmark, in 2001.

From 1988 to 1989, he was a researcher at the Asiago Astrophysical Observatory. From 1989 to 1990, he worked as Engineer in AERITALIA GSS (now Thales Alenia Space). From 1991 to 1997, he worked first as trajectory and system engineer at ESA-ESTEC, mainly in support to the ATV project, and later as coprincipal investigator of the AVS experiment on board A502, the second Ariane 5 test flight. He was also the Vitrociset contractor-ship site manager in 1997. From 1998 to 2001, he was Ph.D. student at the Oersted-DTU Department of the Technical University of Denmark, and visiting researcher at the Institute for Astronomy (IFA) of the University of Hawaii, Hilo, from October 1999 to April 2000. From 2001 to 2004, he was an Associate Professor at the Oersted-DTU Department of the Technical University of Denmark and affiliated to the Center for Planetary Research. In September 2004, he joined ESA-ESTEC as a System Engineer in the Directorate of Earth Observation. He was study manager for the Phase 0 system study and currently System Engineer of the Phase A study of the *MetOp* Second Generation mission.

Maria Belmonte Rivas received the B.S. degree in physics from the Universidad Complutense de Madrid, Madrid, Spain, in 1999 and the M.S. and Ph.D. degrees in aerospace engineering from the University of Colorado at Boulder, in 2007. She has been involved in the analysis of global positioning system signal reflections for ocean altimetry, ocean wind, and the characterization of polar sea ice.

From 2007 to 2010, she worked at the Royal Netherlands Meteorological Institute (KNMI) on the production of daily global sea ice maps using satellite scatterometers. She is currently stationed at the National Center for Atmospheric Research in Boulder, working on atmospheric retrievals from the EOS Aura Infrared Limb Sounder.

Ad Stoffelen was born on February 25, 1962, in The Netherlands. He received the M.Sc. degree in physics from the Technical University of Eindhoven, Eindhoven, The Netherlands, in 1987 and the Ph.D. degree in meteorology on scatterometry from the University of Utrecht, Utrecht, The Netherlands.

He leads a group on satellite wind sensing at the Royal Netherlands Meteorological Institute (KNMI) and is responsible for scatterometer wind products on behalf of EUMETSAT. He is also deeply involved in the European Space Agency's ADM-Aeolus Doppler Wind Lidar mission.

Jos de Kloe studied physics at the University of Utrecht, Utrecht, the Netherlands, until December 1992. After a research project on laser-cooling simulations, and fulfilling his military duty, he started in 1995 with Ph.D. degree work at the Institute for Plasma Physics "Rijnhuizen" in Nieuwegein, The Netherlands. He received the Ph.D. degree in physics from the Technical University of Eindhoven, Eindhoven, The Netherlands, in 2000 with a thesis on "Pellet-plasma interaction in a TOKAMAK."

He worked for one year at the University of Utrecht on the subject of parallelising scientific software. Since October 2000, he has been employed at the Royal Netherlands Meteorological Institute (KNMI) in the Weather Research Division, for European Space Agency (ESA) and national projects. He has worked on building software for simulating scatterometer instruments, and software for (re-)processing actual scatterometer data, and also on implementing software needed to produce an AUTOMETAR (automatically generated weather reports for aviation). For the last five years, he has mostly been involved in the design and development of the wind retrieval processor for ESA's ADM-Aeolus Doppler Wind Lidar satellite mission.